Observations of volcanic earthquakes and tremor at Deception Island - Antarctica

Gerardo Alguacil ([1]), **Javier C. Almendros** ([1]), **Edoardo Del Pezzo** ([3])([4]), **Alicia Garcia** ([2]), **Jesus M. Ibañez** ([1]), **Mario La Rocca** ([3]), **José Morales** ([1]) **and Ramon Ortiz** ([2])

([1]) *Instituto Andaluz de Geofisica, Universidad de Granada, Spain*

([2]) *Museo Nacional de Ciencias Naturales, CSIC, Madrid, Spain*

([3]) *Dipartimento di Fisica, Università di Salerno, Baronissi (SA), Italy*

([4]) *Osservatorio Vesuviano, Centro di Sorveglianza, Napoli, Italy*

Abstract

Deception Island - South Shetlands, Antarctica is site of active volcanism. Since 1988 field surveys have been carried out with the aim of seismic monitoring, and in 1994 a seismic array was set up near the site of the Spanish summer base in order to better constrain the source location and spectral properties of the seismic events related to the volcanic activity. The array was maintained during the Antarctic summer of 1995 and the last field survey was carried out in 1996. Data show the existence of three different groups (or families) of seismic events: 1) long period events, with a quasi-monochromatic spectral content (1-3 Hz peak frequency) and a duration of more than 50 s, often occurring in small swarms lasting from several minutes to some day; 2) volcanic tremor, with a spectral shape similar to the long period events but with a duration of several minutes (2-10); 3) hybrid events, with a waveform characterised by the presence of a high frequency initial phase, followed by a low frequency phase with characteristics similar to those of the long period events. The high frequency phase of the hybrid events was analysed using polarisation techniques, showing the presence of *P* waves. This phase is presumably located at short epicentral distances and shallow source depth. All the analysed seismic events show back-azimuths between 120 and 330 degrees from north (corresponding to zones of volcanic activity) showing no seismic activity in the middle of the caldera. Particle motion, Fourier spectral and spectrogram analysis show that the low frequency part of the three groups of the seismic signals have similar patterns. Moreover careful observations show that the high frequency phase which characterises the hybrid events is present in the long period and in the tremor events, even with lower signal to noise ratios. This evidence suggests that long period events are events in which the high frequency part is simply difficult to observe, due to a very shallow source and/or hypocentral distance higher than that of hybrids, while the tremor is composed of rapidly occurring hybrid events. We propose a possible interpretation for the three groups of seismic events. These may be generated by multiple pressure-steps due to the rapid phase change from liquid to vapour in a shallow aquifer which comes in contact with hot materials. The pressure change can put a crack in resonance or excite the generation of multiple surface waves modes in the shallow layered structure.

Key words *volcanic earthquakes – tremor – Antarctica*

Mailing address: Prof. Edoardo Del Pezzo, Osservatorio Vesuviano, Via A. Manzoni 249, 80123 Napoli, Italy; e-mail: delpezzo@osve.unina.it

1. Introduction

Deception Island (62°59′S, 60°41′W), is the main active volcano of the Bransfield Strait marginal basin, located between the South Shetland Islands and the Antarctic Peninsula (figs. 1 and 2). Its recent eruptions took place in 1848,

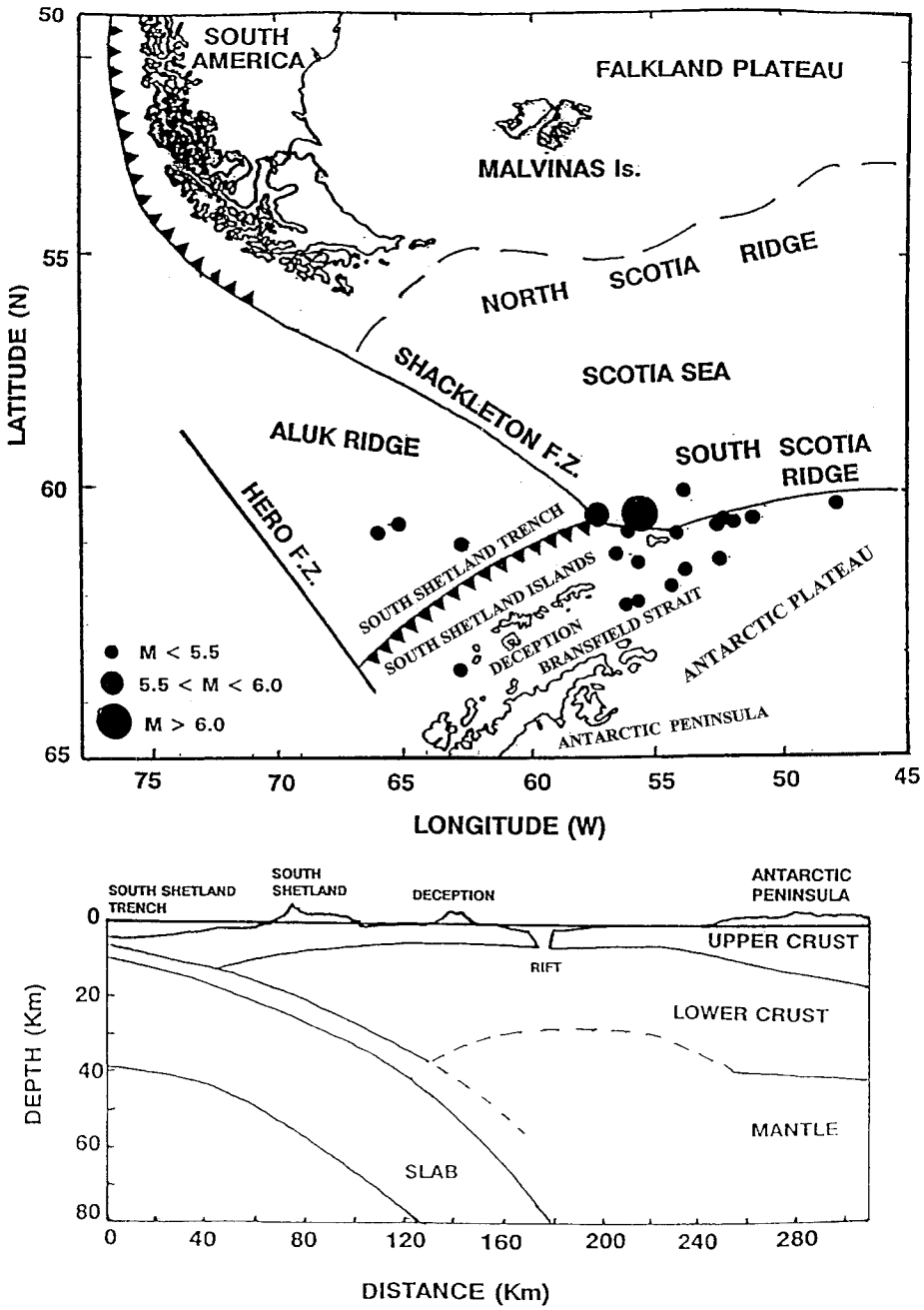

Fig. 1. Tectonic sketch map of the zone between the South Shetland Islands and the Antarctic Peninsula. Deception Island is located in the Bransfield Strait. Black circles represent the epicentral location of the most important earthquakes recorded in the last 40 years (circle size is proportional to the magnitude). On the bottom of the figure a possible tectonic interpretation is reported (from Ibañez *et al.*,1997).

1967, 1969, 1970 and, with more uncertainty, around 1912 and 1917.

The Bransfield Strait is also the site of other volcanoes with evidence of recent activity (Penguin and Bridgeman volcanoes, not reported in the map of fig. 1). A detailed description of the geology, tectonic and dynamics of the Bransfield Strait is reported in Vila *et al.* (1992, 1995), which contain many of the references on this subject. Here we will summarise briefly the main tectonic and geodynamic features of the above mentioned zone. Geophysical data show that the South Shetland Islands lie on a continental plate, bordering to the west with a trench zone which represents the last surviving segment of an old subduction zone which originally extended along the whole margin of the Antarctic Peninsula. The strait zone has been interpreted as a back arc marginal basin, related to the possible subduction of the continental lithosphere toward the southeast, confirmed by the presence of intermediate depth seismicity (Ibañez *et al.*, 1997). A sketch of this situation is reported in fig. 1, taken from Ibañez *et al.* (1997).

Deception Island (fig. 2) was considered a collapse caldera formed by subsidence along an arcuate fault system (Smellie, 1989). More recently Martì *et al.* (1995) pointed out the existence of a tensional stress field with random direction at the surface, compatible with the main direction of the regional stress field. The presence of shallow and confined water-saturated layers (Martini and Giannini, 1988) explain the presence and the chemical composition of low temperature fumaroles throughout the island. An unusual negative anomaly (> 3000 nT) in the zone of the bay (Port Foster, see fig. 2) is in agreement with the interpretation of the gravimetric model in terms of a low-density body beneath the island (Vila *et al.*, 1995). The eruptions which took place in the island of Deception are located along the inner margin of the bay, and all are of the phreato-magmatic type.

Seismicity was observed during several field surveys carried out in the Antarctic summers. It consists of several low-magnitude shocks which have been interpreted by Vila *et al.* (1995) who report all the other references on this subject, as local seismicity possibly connected with the fracture system. Local attenuation studies are in agreement with a shallow magmatic body producing the magnetic anomaly (Vila *et al.*, 1995).

In the last three field surveys carried out at Deception Island by the Spanish group an array of short period seismometers was set up in order to investigate the wave composition, spectral properties and source characteristics of the seismic events which occur at Deception Island. Tectonic seismicity (Ibañez *et al.*, 1997) as well as volcanic events related to local volcanism were recorded. In the present paper we describe these volcanic events, classifying them into three different categories, and interpret the features of the waveforms in terms of source. Such a source may be the same for the three categories, and reasonably may be related to the pressure steps occurring in a shallow aquifer, possibly generated by sudden phase conversions between water and steam. These pressure steps may excite a crack or directly generate the multi-mode surface waves which compose the low-frequency part of the volcanic quake seismograms.

2. Instrumentation and data acquisition

A small aperture seismic array was deployed near the «Gabriel de Castilla» Spanish base on Deception Island during the two Antarctic summers of 1994-1995 and 1995-1996. Configuration was the same for the two surveys (fig. 2). Sensors were 15 vertical MARK L15B with extended response to 1 Hz and 3 three component MARK L4C seismometers. A three component Guralp CMG-3 was set up during the 1994-1995 survey in the same place of one of the three component MARK L4C. The signal of each sensor was amplified, filtered with an antialias analog filter. Groups of 8 channels were cable connected with a PC based, 16 bit, A/D converter. Each channel was sampled at 200 sps rate. We used 3 portable PC to monitor 24 channels. Time synchronisation for each PC was obtained using a GPS signal. Relative coordinates of the array sensors were obtained with GPS positioning. A LTA/STA algorithm was used to record all the events exceeding a threshold triggering the array, while close to the

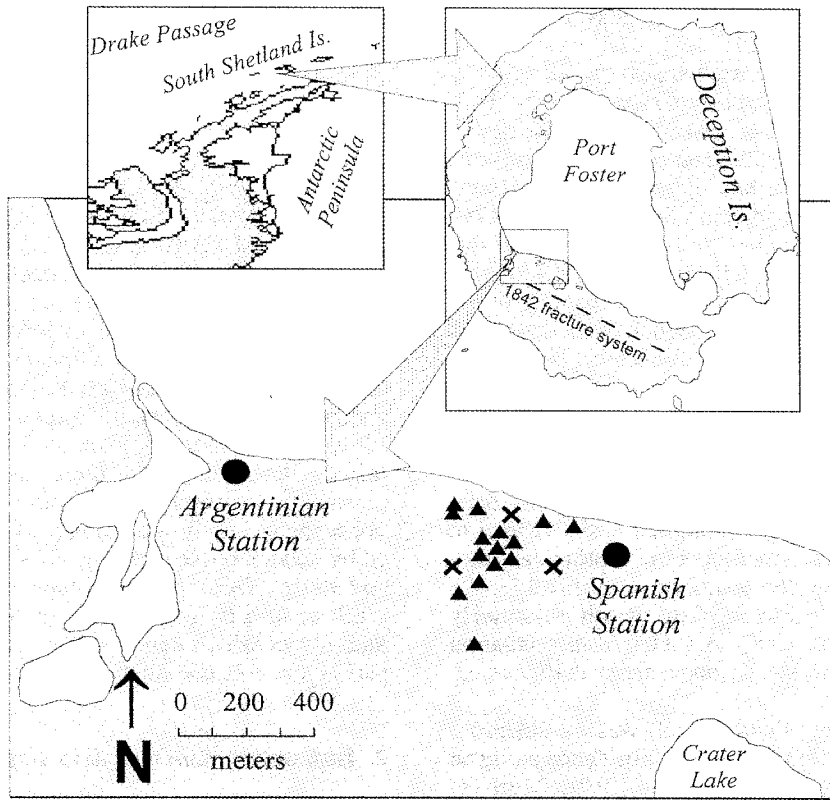

Fig. 2. From the left: location of Deception Island in the Drake Passage. The main feature of Deception Island, and on the bottom, the zone in which the seismic array was set up. Triangles show the position of the array vertical sensors, and crosses the position of the three component sensors.

«Gabriel de Castilla» Spanish base an analog station was set up with paper recording on a «helicorder type» drum, which was used as a continuous monitor. We recorded about 600 seismic events during the first survey and more than 1000 in the second. Many triggered events correspond to volcanic tremor, as we could check looking at the monitor drum.

Data records contain a wide variety of seismic signals, which can be grouped into tectonic regional earthquakes and local events. Tectonic earthquakes are discussed in a separate paper (Ibañez *et al.*, 1997). Local events linked to the volcanism are described and discussed in the present paper.

3. Event classification

Seismic records which triggered the array at all the stations were visually inspected and classified on the basis of the waveform. Tectonic events show clear *S* phases, and were easily grouped using some experience. They are described in Ibañez *et al.* (1997), as already indicated. The rest of the seismic events are more closely related to the volcanic activity. They were grouped into categories, on the basis of waveform. The most populated categories were three: 1) long period event; 2) hybrid events, and 3) tremors. An example of the most characteristic events is reported in figs. 3a-c, together with their Fourier spectra.

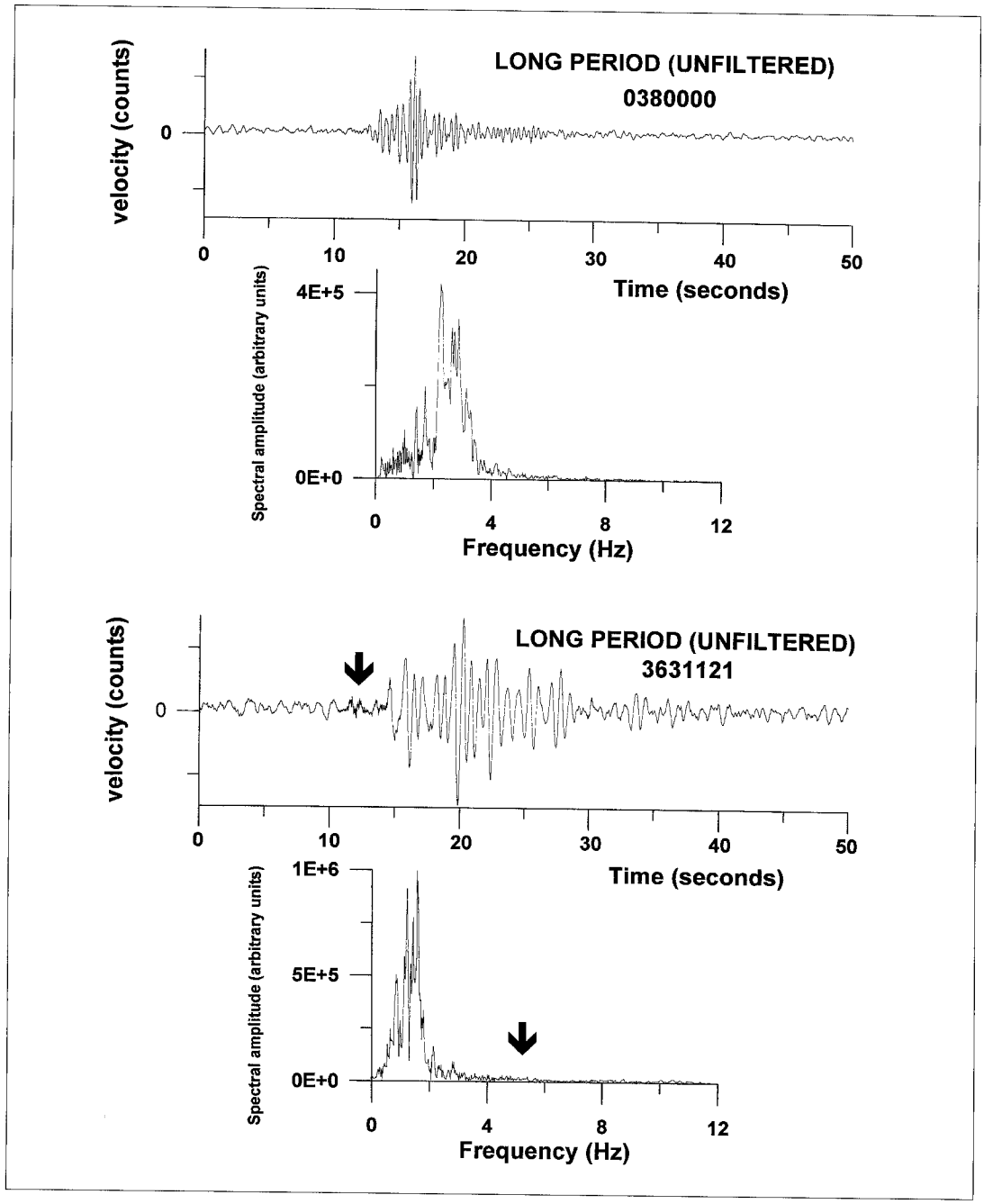

Fig. 3a. Two examples of typical long period events with their spectra. Note the high frequency phase, with low amplitude, marked with an arrow on the event reported on the third panel from the top and on its spectrum in the bottom panel.

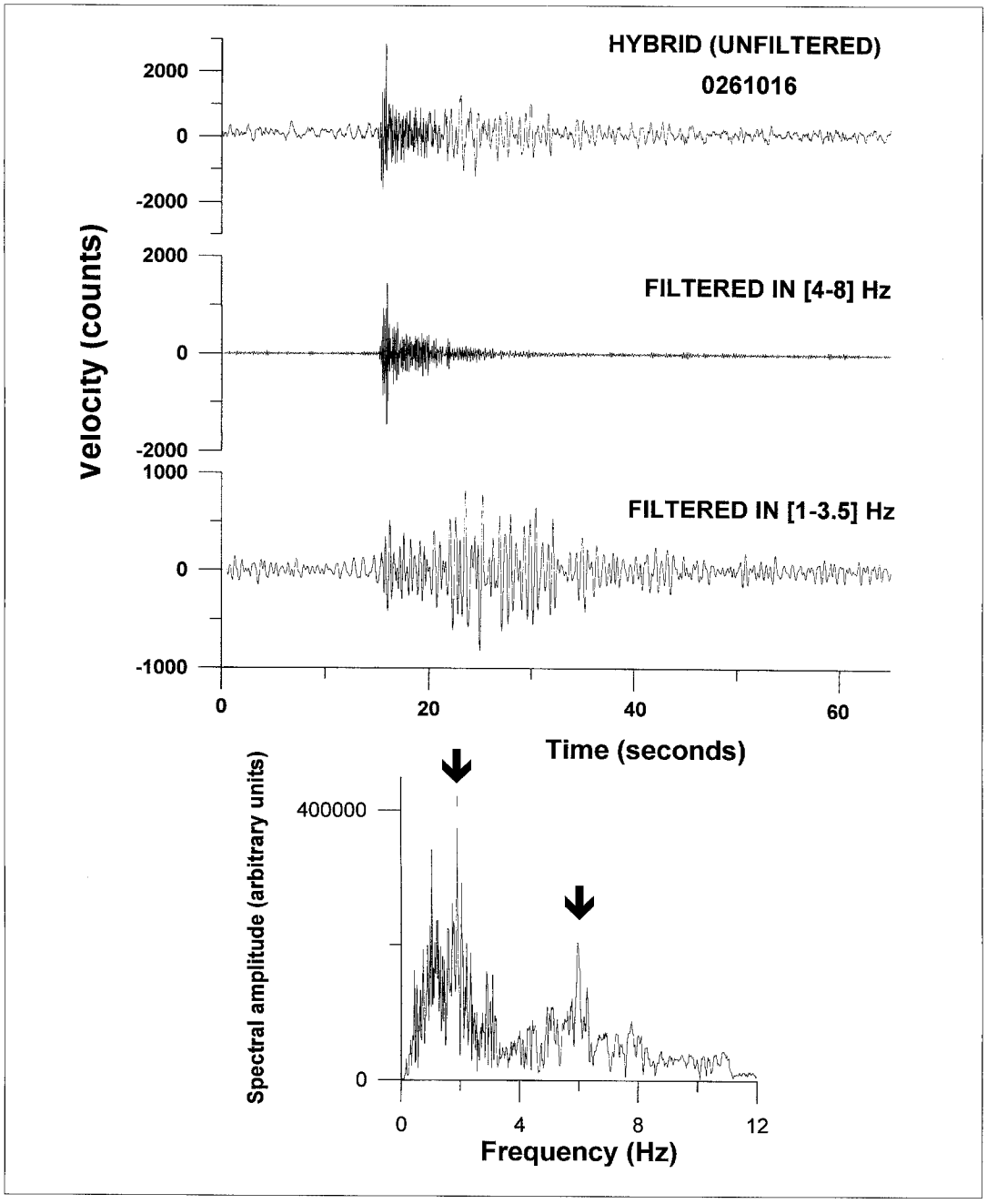

Fig. 3b. An example of a hybrid event (top). The unfiltered seismogram, the seismogram filtered in the 4-8 Hz band and the seismogram filtered in the 1-3.5 Hz band. In the spectrum (bottom) arrows indicate the predominant peaks at low and high frequency.

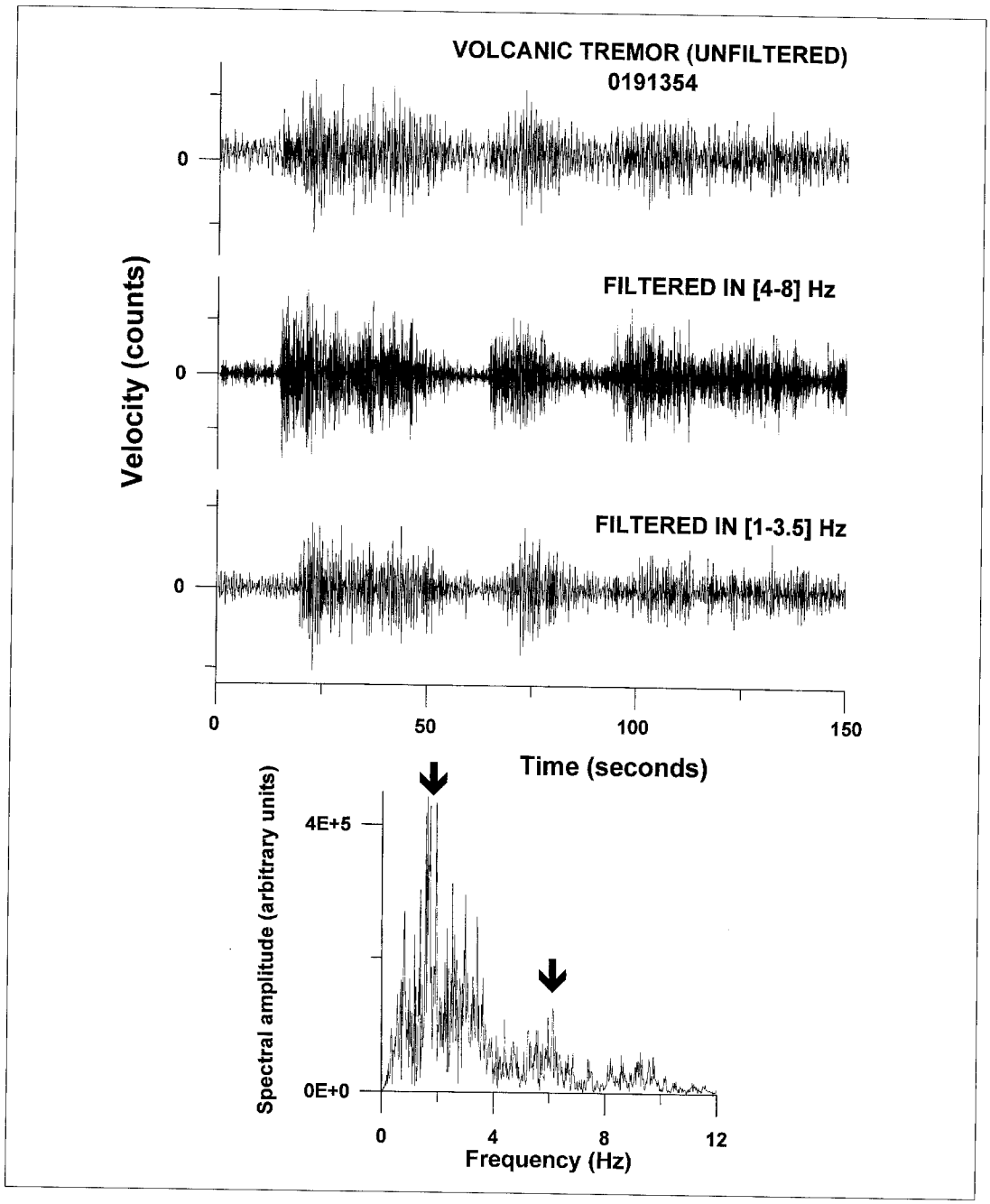

Fig. 3c. An example of volcanic tremor. From the top: the unfiltered trace, filtered in the 4-8 Hz band, filtered in the 1-3.5 Hz band and the frequency spectrum (bottom). In the spectrum arrows indicate the predominant peaks at low and high frequency.

Long period events show a seismogram consisting of a wave packet with an almost constant predominant frequency. These events show a lack of distinct phases, except for the most energetic ones, which show a small amplitude initial phase composed of a frequency higher than the rest of the seismogram, lasting for one or two seconds. In this last case the Fourier spectrum shows two distinct peaks, one at about 2 Hz, with higher energy, and the second at 4-5 Hz with smaller amplitudes, corresponding to the initial phase. For most of the long period events the high frequency initial phase is indistinguishable from the noise. They have waveforms similar to those of the long period events discussed by Power *et al.* (1994), recorded at Redoubt volcano, Alaska.

Hybrids show the peculiar characteristic of a distinct high frequency phase, beginning with the first onset of the earthquake and lasting some seconds, followed by a low frequency wave-train. The spectral characteristics of this kind of events are similar to those of the long period events, with an additional peak around 8 Hz corresponding to the first phase at high frequency.

Tremors are continuous wave-trains, lasting several minutes (up to hours or days). Due to the limited duration of the signals triggered by the LTA/STA algorithm we can investigate the tremor signals which triggered the array, with a duration not greater than 180 s. The tremor waveforms, as visually inspected on the continuous paper monitor, do not change apparently throughout the tremor episode. Their spectra show that most energy is in the range between 1 and 5 Hz, generally showing two distinct bands, the first between 1 and 3 Hz, and the second at more than 4 Hz. It is noteworthy that in several cases a hybrid event (fig. 5) was recorded by the array in the time between two episodes of volcanic tremor.

4. Method for determination of back-azimuth and apparent velocity

We used the zero-lag cross-correlation technique to measure the back-azimuth and slowness for any distinct phase of the volcanic events classified as tremor, long period or hybrids.

In the hypothesis of a plane wave which crosses the array of seismic stations with a slowness vector $\boldsymbol{p}$, let t_{ij} the travel time difference between the station i and j of the array. It will result

$$t_{ij} = p_x \Delta x_{ij} + p_y \Delta y_{ij} + p_z \Delta z_{ij}$$

where p_x, p_y and p_z represent the coordinates of the slowness vector. If the seismic traces are translated by the quantity t_{ij} measured respect to a given reference station, it will result that the so called «zero-lag cross-correlation» coefficient (Frankel *et al.*, 1991), given by

$$c_{i,j} = \frac{\sum_{k=1}^{M} A_k^i \cdot A_k^j}{\sqrt{\sum_{k=1}^{M} (A_k^i)^2 \cdot (A_k^j)^2}} \qquad (4.1)$$

where A stands for seismogram amplitudes, k is the time sample and M is the number of time samples, is maximum for each couple of stations i, j. It is clear that $c_{ij} = c_{ji}$ and if we have N seismograms it will result $N(N\text{-}1)/2$ different values of c_{ij}. Also, the average of all the coefficients c_{ij}, $< c_{ij} >$, will be maximum.

In the present paper we use a grid search to find, for each seismogram recorded at the array of stations, the slowness vector which maximises $< c_{ij} >$. The procedure is described in detail in Del Pezzo *et al.* (1997), and here briefly in the next six steps.

1) We fix the value of the slowness on a grid.

2) We calculate the corresponding set of t_{ij} and then we shift the seismograms.

3) We calculate the zero-lag cross-correlation for each couple and then the average.

4) We repeat the cycle starting again from step 1. In this way we obtain the average zero-lag cross-correlation for all the values of the slowness fixed on the grid: $C(p_x, p_y)$.

5) We select the maximum of $C(p_x, p_y)$ which will correspond to the «true» slowness vector.

6) The back-azimuth is obtained by the formula $\phi = \arctan(p_x/p_y)$, and the apparent velocity by $v_a = 1/(p_x^2 + p_y^2)^{0.5}$.

A similar procedure was used by Frankel *et al.* (1991) and by Mori *et al.* (1994).

It is noteworthy that if the grid is obtained using constant Δp increments, the resolution decreases for increasing apparent velocities. To avoid this effect we built the grid increasing step by step $\phi = \arctan(p_x/p_y)$, by a constant quantity $\Delta\phi$; $p = (p_x^2+p_y^2)^{0.5}$ was increased by Δp in such way that $\Delta p/p$ remains constant step by step. In this way we obtain a good compromise between resolution and computer speed.

We examined two main sources of errors: the errors due to the sampling rate of the time series, the array geometry and the grid search; and the errors generated by the seismic noise and by the lack of coherence of the signal through the array.

a) *Space and time sampling and grid search* – The seismograms were digitised at a sampling period $T_0 = 0.005$ s. For this reason, when the seismograms are shifted to calculate the zero-lag cross-correlation, this time shift has to be an integer multiple of T_0: $T_i = n_i T_0$ where n_i is an integer. The percent error generated by this approximation decreases with increasing T_i, or with decreasing apparent velocity. This effect fixes the lower limit of the Δp step in the grid, say Δp_{min}. Δp_{min} can be for this reason reasonably considered as an estimate of the error due to the above described effect.

b) *Seismic noise* – In order to evaluate the effect of the noise on the estimate of the zero-lag cross-correlation we selected a time window of the seismogram, before the arrival of the *P* phase, containing only noise. Then we estimated the cross-correlation for the signal and for the noise window (non normalised by the denominator of relationship (4.1). If we denote with $< C_r >$ the cross-correlation of the noise window averaged over the whole p_x-p_y grid, and C_s the maximum of $C(p_x, p_y)$ for the signal, then an estimate of the percent error on the maximum value of the cross-correlation can be given by

$$\Delta C/C = < C_r > / C_s.$$

The uncertainty on apparent velocity and back-azimuth can be obtained selecting the values p_x and p_y on the grid for which results

$$C(p_x, p_y) > C_s - \Delta C.$$

This points define an «uncertainty zone» which can be used to evaluate the uncertainty on back-azimuth and apparent velocity. We noted that the zero-lag cross-correlation between couples of seismograms never approaches to the value of unity, which means perfect similarity between the waveforms. This effect is due to the lack of coherence through the array, probably generated by local site effects. We weighted empirically this effect defining an additional error $\Delta C = (1 - C_{max})/n$ where $n = N(N-1)/2$ is the number of couples of stations on which we calculate the zero-lag cross-correlation. In this way ΔC is close to 0 when the similarity between the signals is maximum. Finally, we calculate the mean squared of the errors due to the lack of coherence and due to the noise.

We tested the ZLC method using a synthetic wavelet (Del Pezzo *et al.*, 1997) which was propagated through the array AB. We added to the signal a random noise in order to test the stability with different signal to noise ratios. An example is reported in fig. 4, obtained with a signal to noise ratio of 10, close to that measured on the real signals analysed at the end of the coda. Errors on the estimate are less than 5 percent, and the test data are well reproduced by the method. A further test was made by applying the high resolution and beamforming spectral methods, described by Capon (1969), and widely used in literature, to the same synthetic signal (fig. 4). In order to make this further check significant we utilised a time window of 64 points (a power of two), of the same order of duration as those utilised for real data using the ZLC. Results show that using these two spectral methods, the azimuth is always very well reproduced, while apparent velocity is always overestimated. The estimate obtained using the two spectral methods suffers for the limited number of data points, indicating that for high frequency seismograms and short duration seismic phases they are practically impossible to apply.

5. Data analysis and results

We selected 12 hybrids, 56 long-period events and 14 volcanic tremors on the basis of the best signal to noise ratio. On the basis of the results from spectral analysis we do not observe a very unique spectral shape. For example, some long-

Table I. Frequency band used for filtering.

Event type and name	Low-frequency band (Hz)	High-frequency band (Hz)	Event type and name	Low-frequency band (Hz)	High-frequency band (Hz)
HY-0020536	1.0-2.5	3.0-6.0	LP-0380102	1.0-3.5	–
HY-0021039	1.0-2.0	3.0-6.0	LP-0380252	1.0-2.5	–
HY-0040435	1.0-2.0	4.0.8.0	LP-0380637	1.0-2.5	–
HY-0071026	1.0-2.0	6.0-10.0	LP-0381048	1.0-2.5	–
HY-0210112	1.0-2.0	6.0-10.0	LP-0381241	1.0-2.0	–
HY-0261016	1.0-3.5	4.0-8.0	LP-0381331	1.0-2.0	–
HY-0351943	1.0-2.5	4.0-8.0	LP-0381434	1.0-2.0	–
HY-0391622	1.0-3.5	4.0-8.0	LP-0390446	1.0-2.5	–
HY-0521246	1.0-2.0	4.0-8.0	LP-0390604	1.0-2.5	–
HY-3631158	1.0-2.5	3.0-6.0	LP-0390741	1.0-2.5	–
HY-3631256	1.0-2.0	3.0-6.0	LP-0391459	1.0-3.5	–
HY-3641716	1.0-3.5	4.0-8.0	LP-0391559	1.0-2.5	–
LP-0021444	1.0-2.0	–	LP-0391945	1.0-3.5	–
LP-0040646	1.0-2.0	–	LP-0400336	1.0-3.5	–
LP-0070040	1.0-2.0	–	LP-0400343	2.0-3.5	–
LP-0120003	1.0-3.5	–	LP-0400502	1.0-3.5	–
LP-0361704	1.0-2.5	–	LP-0400836	2.0-3.5	–
LP-0361957	1.0-2.0	–	LP-0401206	2.0-3.5	–
LP-0362053	1.0-3.5	–	LP-0401710	2.0-3.5	–
LP-0362055	1.0-3.5	–	LP-0411705	1.0-2.0	–
LP-0362133	1.0-3.5	–	LP-0450312	1.0-2.0	–
LP-0362236	1.0-3.5	–	LP-3602051	1.0-2.0	–
LP-0362322	1.0-2.5	–	LP-3631121	1.0-2.0	–
LP-0370107	1.0-2.0	–	LP-3631949	1.0-2.0	–
LP-0370211	1.0-2.0	–	LP-3632051	1.0-2.5	–
LP-0370355	1.0-2.0	–	LP-3640919	1.0-2.0	–
LP-0370401	1.0-3.5	–	LP.3641049	1.0-2.5	–
LP-0370716	1.0-2.0	–	TR-0191257	1.0-2.5	4.0-8.0
LP-0370858	1.0-2.5	–	TR-0191326	1.0-2.5	4.0-8.0
LP-0371019	1.0-2.5	–	TR-0191348	1.0-3.5	4.0-8.0
LP-0371120	1.0-3.5	–	TR-0191354	1.0-2.5	4.0-8.0
LP-0371557	1.0-3.5	–	TR-0191456	1.0-2.5	4.0-8.0
LP-0371755	1.0-2.5	–	TR-0191525	1.0-3.5	6.0-10.0
LP-0372245	1.0-3.5	–	TR-0191702	1.0-3.5	4.0-8.0
LP-0372334	1.0-3.5	–	TR-0201544	1.0-3.5	4.0-8.0
LP-0372349	1.0-3.5	–	TR-0201743	1.0-3.5	4.0-8.0
LP-0380000	1.0-3.5	–	TR-0201818	1.0-3.5	4.0-8.0
LP-0380017	1.0-3.5	–	TR-0201917	1.0-3.5	4.0-8.0
LP-0380044	1.0-3.5	–	TR-0452227	2.0-4.0	–
LP-0380048	1.0-3.5	–	TR-3581928	1.0-2.0	4.0-8.0
LP-0380059	1.0-3.5	–	TR-3631253	1.0-2.5	3.0-6.0

periods presented a unique peak centred around 2.5 Hz, while others had this peak located around 1.5 Hz and others show both peaks. At high frequency a multiplicity of spectral peaks was mainly observed in the 4-8 Hz frequency band. Due to this fact, we used for filtering a frequency band that depends on the visual appearance of the Fourier spectrum. In table I we report the frequency bands used for all the analysed events.

After filtering we applied the zero-lag cross-correlation method to the filtered seismograms in order to determine the apparent slowness across the array and the back-azimuth to the associated source. We used a moving window with a length in time domain which depends on the value of the lowest observed peak frequency in the filter band (see table II for details), in order to use always about 2 periods in each window.

We started at the pre-event noise and stopped into the late coda. For each step we evaluated back-azimuth and apparent slowness. Errors in azimuth result smaller than 10 degrees in azimuth and of the order of 10 percent in slowness for correlation higher than 0.7, evaluated using the above described method. An example of this analysis for each of the three event types is reported in figs. 4, 5 and 6.

Table II. Moving window length corresponding to each frequency band reported in table I.

Frequency band (Hz)	Window length (points)
1.0-2.0	300
1.0-2.5; 1.0-3.5	200
2.0-3.5	160
3.0-6.0	100
4.0-8.0; 6.0-10.0	80

For the low-frequency band of the volcanic tremor we observe that the windows with the highest value of zero-lag cross-correlation show constant back-azimuth and apparent velocity. The

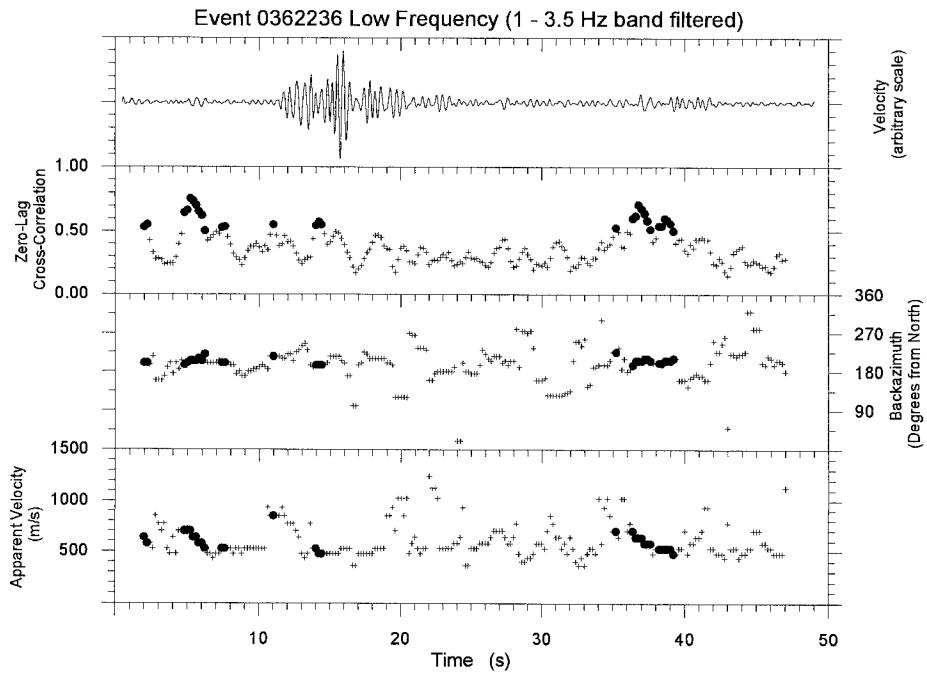

Fig. 4. The ZLC method applied to a low-frequency event. The black dots indicate ZLC values greater than 0.5.

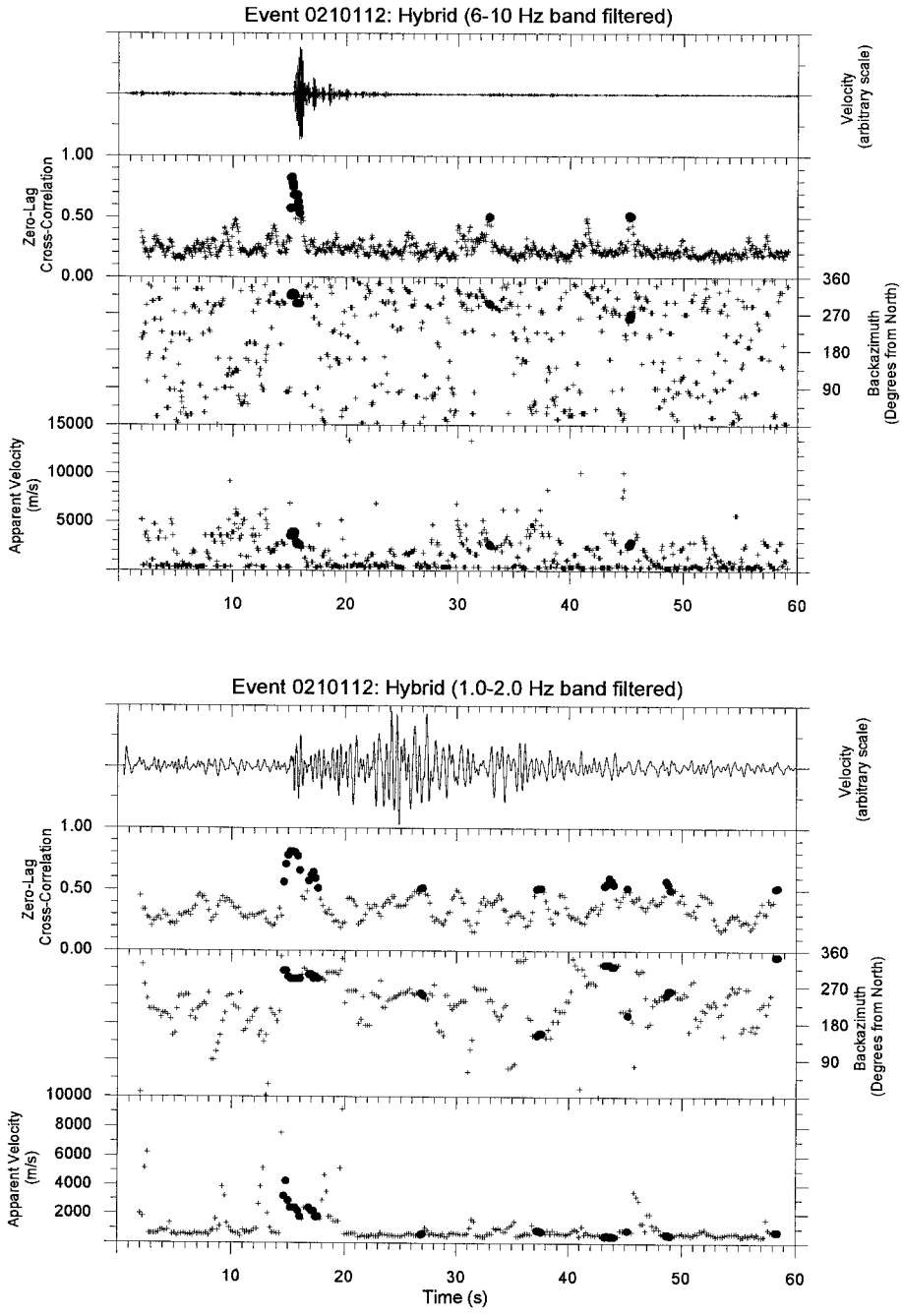

Fig. 5. The ZLC method applied to a hybrid event. The upper four windows show the results obtained for the seismogram filtered between 6 and 10 Hz, while the other four windows show the results for the same event filtered between 1 and 2 Hz. The black dots indicate ZLC values greater than 0.5.

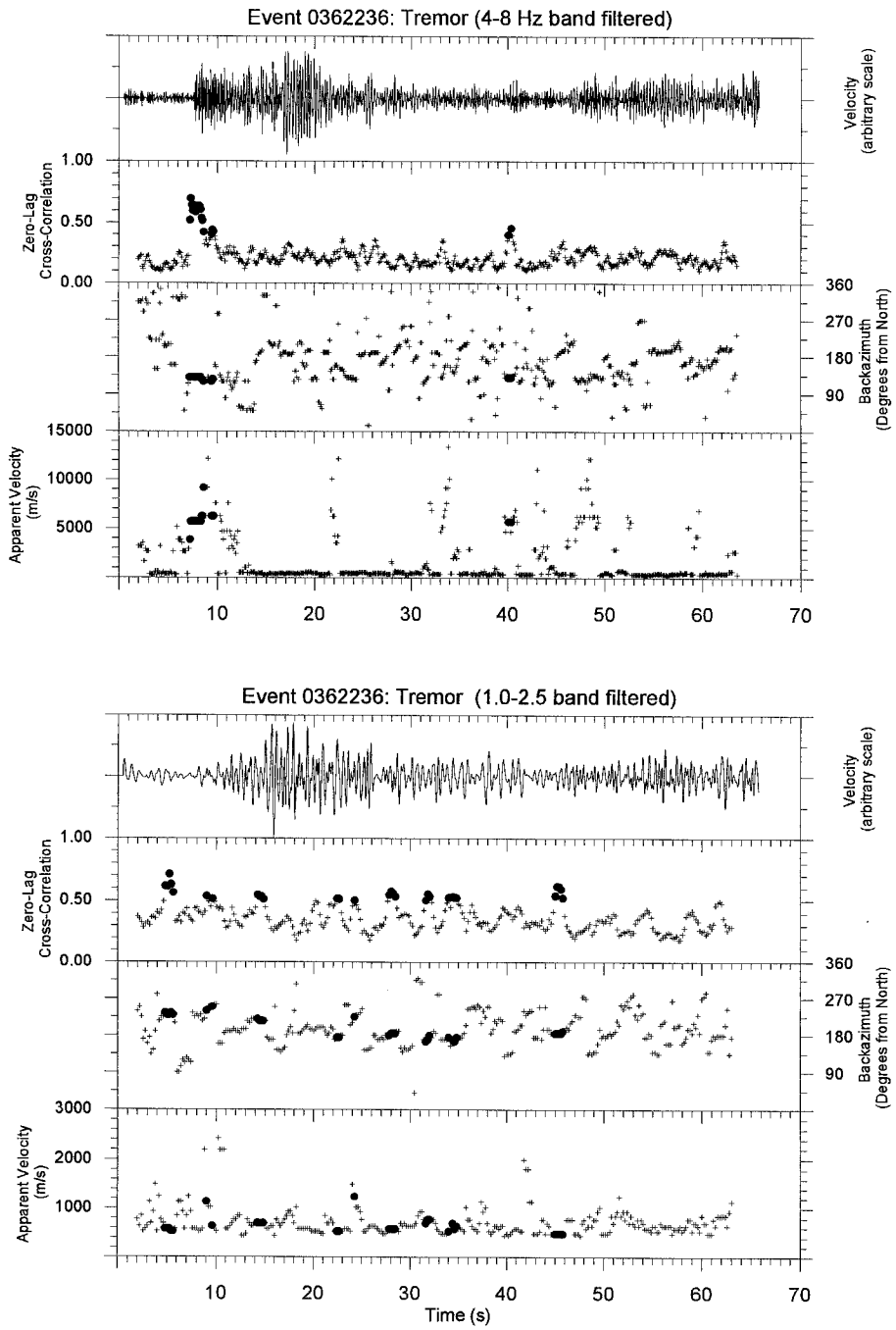

Fig. 6. The ZLC analysis applied to a tremor sample, filtered between 4-8 Hz (the upper four windows) and 1-2.5 (the lower four).

same volcanic tremor samples, filtered at high frequency, generally show a back-azimuth value different from that observed in the seismogram filtered at low frequency; when correlation is high, we observe the same back-azimuth. Moreover the apparent velocity for the seismogram filtered in the high frequency band is higher (up to 6 km/s) than that observed in the low-frequency band. This was also observed by Goldstein and Chouet (1994) at Kilauea volcano.

The hybrid events show a high correlation for the first phase in the high frequency band, corresponding to apparent velocities up to about 4 km/s, and high correlation in the windows corresponding to the low frequency wave-packet which follows the first phase. This last wave packet arrives at the array with low apparent velocity and with back-azimuth which are often different from that of the first phase.

The long period events show a quasi-monochromatic spectral content (1-3 Hz peak frequency) and a duration up to about 30 s. They often occur in small swarms lasting from several minutes to some days. The back-azimuth and slowness for the time windows with high zero lag cross-correlation, remain constant along the seismogram.

The slowness vector pattern for a selection of the whole data set, based on the signal to noise ratio, is represented in figs. 7, 8 and 9. We plot the slowness vector for the three types of events, as follows:

a) *Hybrids* – We select the time window corresponding to the first phase and the time window corresponding to the low frequency phase of hybrids with the maximum correlation.

b) *Long period events* – We select the window with the highest correlation for the long period events.

c) *Tremor* – We select the windows corresponding to the phases with the highest correlation (> 0.7) in the tremor, in the low and in the high frequency band.

We clearly observe that the high frequency phases have higher apparent velocity than the low frequency ones, and that most signals come from the south-west sector. For hybrids the high frequency phase comes from a direction different from that the low frequency phase, which as already described, appears some sec-

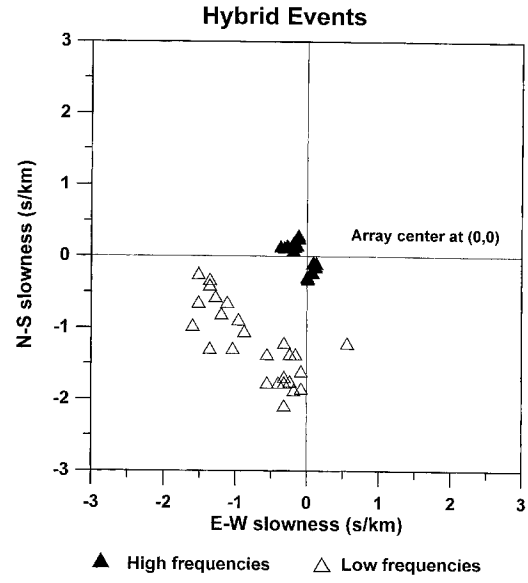

Fig. 7. Distribution of the slowness components for the first phase of the hybrid events (black triangles, high frequency) and for the window with the highest correlation inside the low-frequency phase (empty triangles, low frequency).

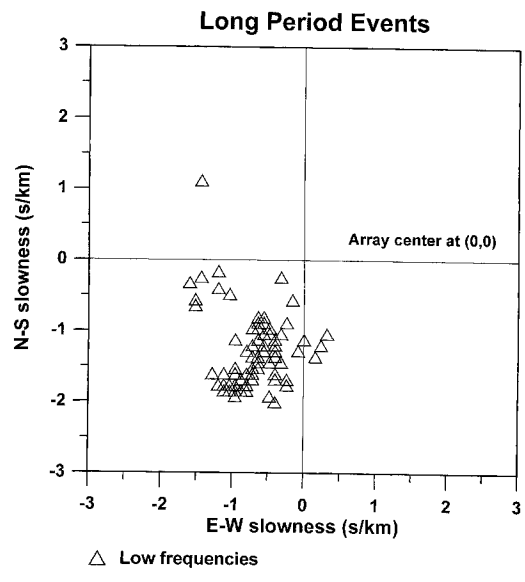

Fig. 8. Distribution of the slowness components (for the time window with the highest correlation) for the long period events.

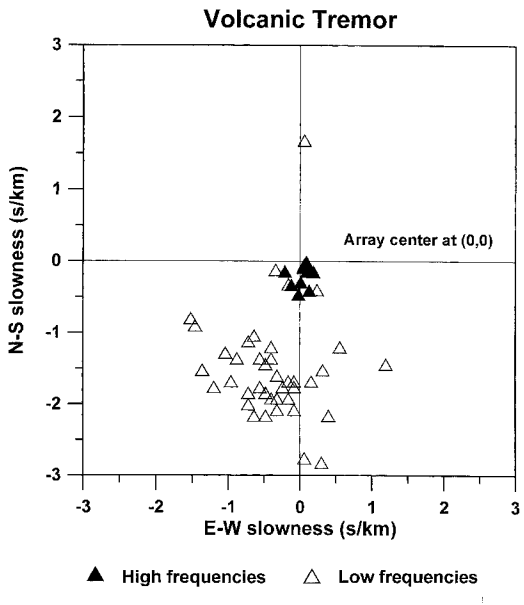

Fig. 9. Distribution of the slowness components for the tremor. We represent the values with ZLC value greater than 0.5 obtained in the low frequency band (filter central frequency below 4 Hz, empty triangles) and in the high frequency band (filter central frequency above 4 Hz, black triangles)

onds later on the seismogram. We are confident that this result is not produced by possible bias in the methodology. A test carried out on a selection of the data set with a different technique (MUSIC algorithm; Goldstein and Chouet, 1994) yielded the same results. In fig. 10 we show the distribution of the back-azimuths in the low and high frequency separately for all the analysed events. Two main directions (145° and 330° from north) were observed for the high frequency phase of hybrids. The 145° direction is coincident with the directions obtained for tremors at high frequency. An almost unique direction (about 200°) was observed for all the low-frequency phases.

6. Particle motion pattern

We studied the particle motion pattern at the three component stations of the array for the best recorded events for each of the three classes. The three components of the ground motion were rotated in the direction of the projection of the wave vector to the surface, obtained by the array analysis. For each seismic event, we fixed the wave vector solution with maximum coherence. In this way we obtained the radial and the transversal component. The main evidence is that the particle motion pattern for the first phase (high frequency) of hybrids is strongly rectilinear in the vertical direction. As this phase comes to the array with a high apparent velocity (see fig. 7), indicating an incidence close to the normal to the horizontal plane, this phase can be interpreted as a *P*-wave (see fig. 11a). As shown in the same figure, the transverse-radial particle motion plot shows no clear phases with particle

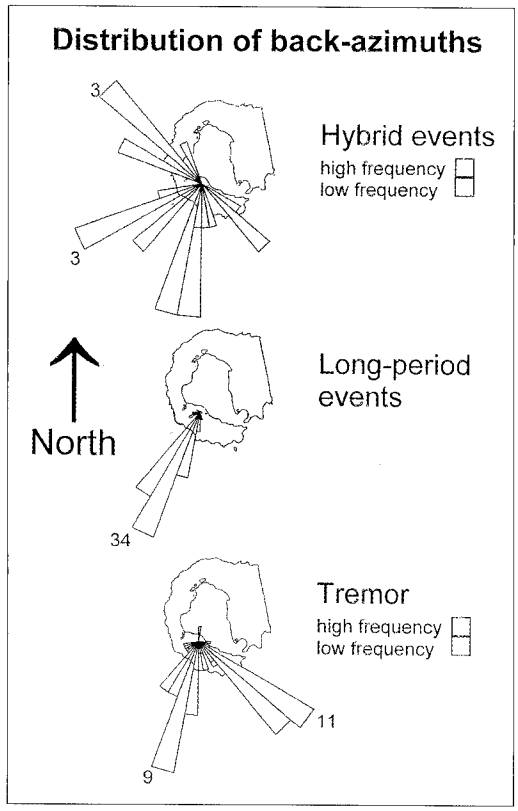

Fig. 10. Distribution of back-azimuths for the three analysed types of events for high and low frequency.

motion normal to the wave vector in the time window corresponding to the arrival of the high frequency wave train for hybrids. This indicates the absence of shear waves. The particle motion pattern for the secondary long period phase which characterises the hybrid events (fig. 11b) shows that this phase contains no clear particle motion in the transversal direction. This excludes a predominant *S*-wave (or Love) composition for this phase. Due to the mixed character of the particle motion pattern and to the low value of the apparent velocity measured at the array for those phases, in agreement with the typical values of the surface wave velocity, we make the hypothesis that this low-frequency phase is mainly composed of Rayleigh-waves.

The tremor samples, filtered at low frequency (fig. 11c), are characterised by a complex particle motion pattern, similar to that found for the low-frequency phase of the hybrids. At high frequency (fig. 11d), the tremor shows some correlated arrivals, as already shown. The particle motion patterns for the correlated arrivals are composed of wave packets characterised by a highly linear particle motion, lasting from 0.5 to 2.5 s, possibly *P*-waves. Particle motions with a clear transversal direction (shear wave phases) were never observed inside these wave packets. It is noteworthy that the hybrid high-frequency initial phases and the high-frequency phases of the tremor samples share a similar particle motion pattern. Moreover the low-frequency events show the same particle motion characteristics as the low-frequency phase in the hybrids and tremor. Due to the low number of 3D stations (3) available, it was impossible to apply array polarisation techniques to the present data. A check of the results obtained using the simple particle motion pattern analysis was performed on some selected data, calculating the rectilinearity parameter from the covariance matrix (Montalbetti and Kanasevich, 1970), obtaining comparable results.

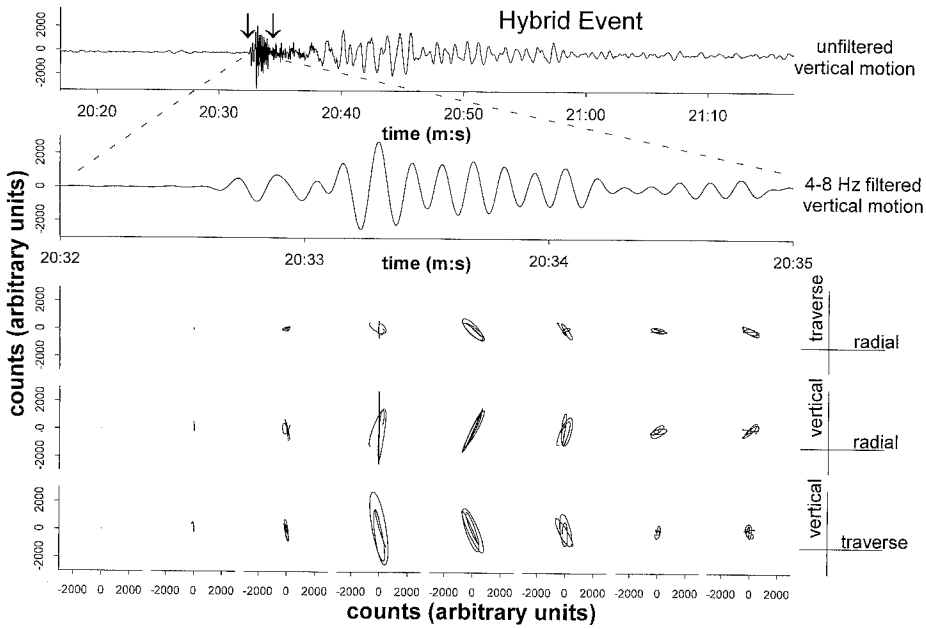

Fig. 11a. Particle motion pattern for the high-frequency phase of a selected hybrid event. In the top panel: the unfiltered trace (vertical component). The two black arrows delimit the analysed time window. In the second panel: the filtered signal. In the three bottom panels: the particle motion plots in the radial-transversal, in the vertical-radial and in the vertical transversal reference.

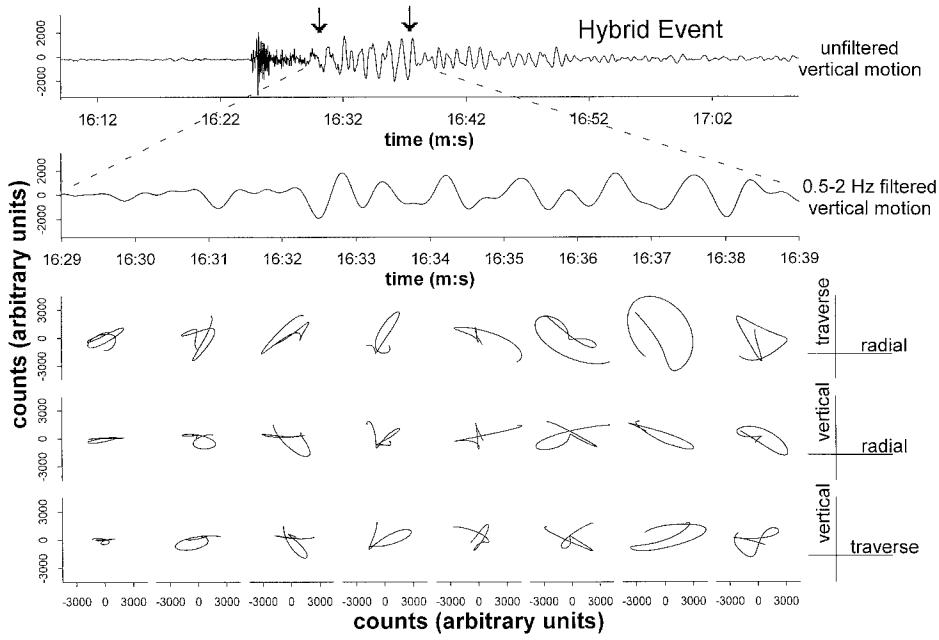

Fig. 11b. The same as fig. 11a for the low frequency part of the hybrid event.

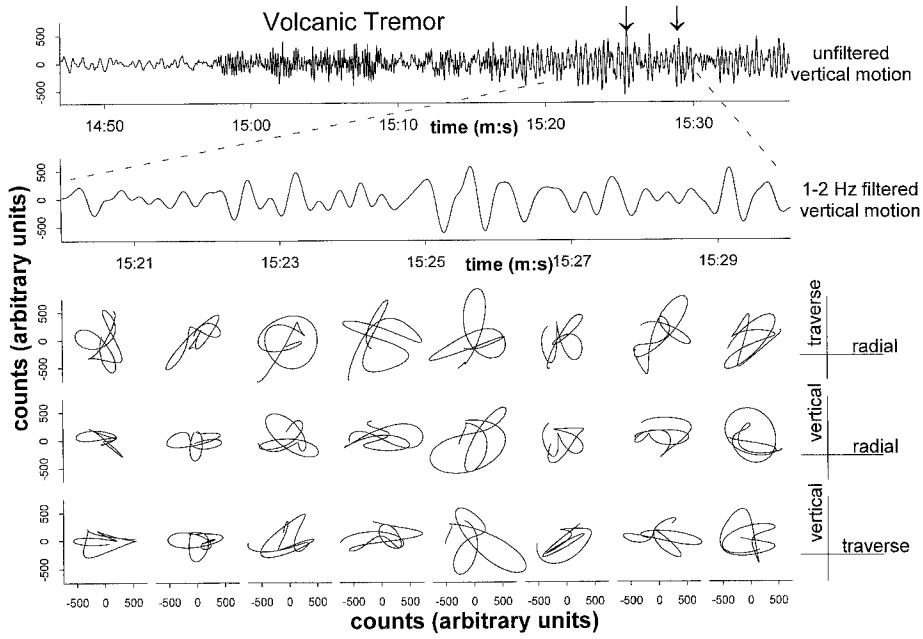

Fig. 11c. The same as fig. 11a for the volcanic tremor (low frequency.)

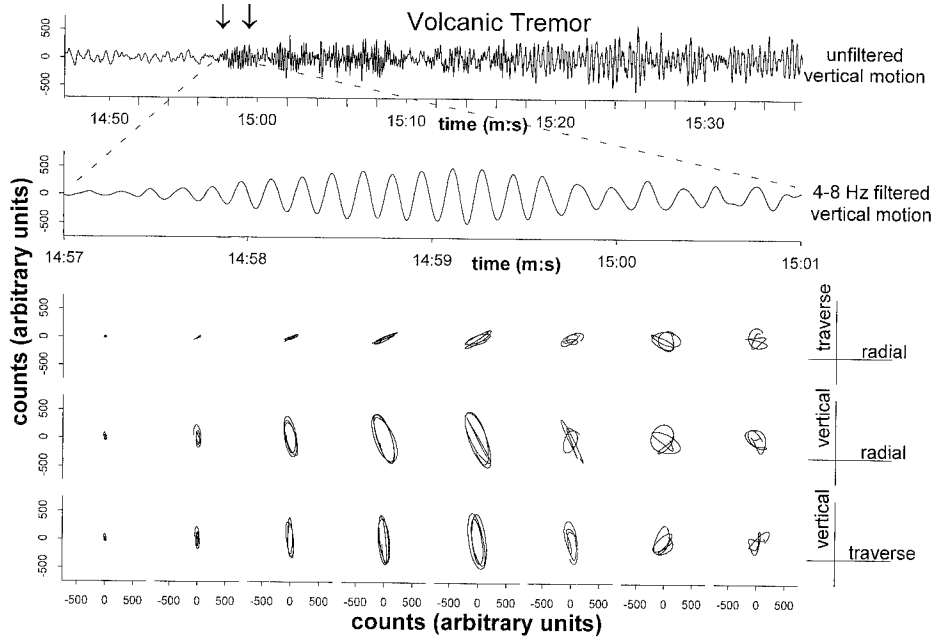

Fig. 11d. The same as fig. 11a for volcanic tremor (high frequency).

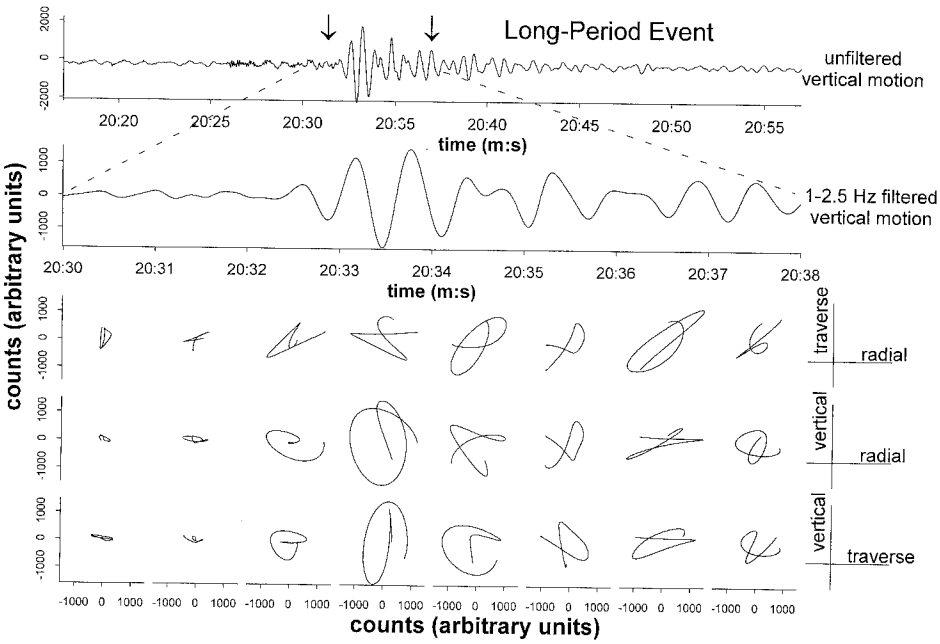

Fig. 11e. The same as fig. 11a for a long period event.

7. Discussion

The main evidence from the array analysis carried out on the volcanic events at Deception Island can be summarised as follows:

1) Three main classes of events with apparently different waveforms were recorded: hybrids, long-period and tremor.

2) Coherent *P*-wave pulses with peak frequency around 4-8 Hz in the first phase of the hybrid events and inside the tremor wave train were observed.

3) No clear *S*-wave pulses in any of the three classes of events were observed.

4) The back-azimuths measured for the well correlated low-frequency phases of hybrids, low-frequency events, and tremors are all in the same S-E quadrant. Moreover their particle motion pattern is in agreement with a surface wave composition.

5) A group of hybrid events show the first phase which shares the same back-azimuth and slowness pattern as the high frequency phases for a group of tremor events.

6) The high frequency phases for the tremor and for the hybrid events show different back azimuth and slowness than the low-frequency phases inside the same seismogram.

7) Sometimes a high frequency phase, similar to that of hybrids but with smaller amplitude, is recorded at the beginning of the long period events.

The above evidence can be interpreted, in a speculative way, in terms of a source related to the presence of the shallow aquifer which presumably is in contact with high temperature rocks. In such a situation water and steam may stay in a ordinary situation of stable thermodynamical equilibrium. When the weather changes from the Antarctic winter to the spring, giving rise to an increase in the water volume into the aquifer, due to the thaw, the equilibrium can be locally altered. The thaw occurs quite rapidly in Deception Island, and in a time interval not longer than some weeks, the sea water of the bay thawed completely, as observed by many people surveying the zone in that time period.

The shallow cracks filled by water may be the cause of the volcanic shocks recorded at Deception. The mechanism could be the crack resonance (Chouet, 1992) excited inside the crack by the exploding or imploding bubbles of steam (Lu *et al.*, 1990). Reaching new equilibrium states could be accompanied by sudden phase changes from liquid water to vapour, giving rise to the crack resonance phenomena, which could occur clustered in time (tremor) or isolated (hybrids).

This kind of crack resonance has been modelled by Chouet (1986, 1992) and Morrissey and Chouet (1997). The model is based on experimental observations of long-period events and tremor. The long-period events are considered a sort of impulse response of the complex tremor generating system. The crack waves are dispersive and their spectral shape depends on many parameters such as crack geometry, the bulk modules of the fluid which permeates the crack, the solid rigidity and the crack thickness. It is a difficult task to invert from the spectra the dynamical crack parameters without a good knowledge of the spatial position and orientation of the crack with respect to the recording array, as in Deception. The crack model is in good agreement with the experimental observations: the high frequency phase, observed at the beginning of the hybrids and sometimes of the long-period events, can be related to the triggering phenomena (the phase change) which excite the crack resonance.

It is noteworthy that the model is not unique. A buried explosion (in the aquifer) would produce in fact strong compressional waves at the source together with Rayleigh waves at the discontinuities, mainly at the surface. This hypothesis is also in agreement with the observations carried out for hybrids and tremor events at Deception Island. In fact both show distinct compressional phases followed by long period Rayleigh type wave-trains. The tremor could be viewed as a superposition of hybrid events, each produced by an explosion in the aquifer. The long period events, as already described, are proceeded by an high frequency phase, characterised by low amplitudes, of the order of those of the pre-event noise. This last could be interpreted, in this alternative model, in the same way for tremor and for hybrids, by a sudden explosion (or implosion) in the shallowest layers. The higher attenuation present in the surface could

be responsible for the observed lower amplitude, which, in some cases, could be equal to or lower than that of the background noise. In this case we would observe the low-frequency events.

This two alternative interpretations are at moment only qualitative, and a more quantitative approach to synthesise the waveforms of the recorded signals is in progress.

Difficult to explain is the different back-azimuth measured for the high and low frequency phase of the hybrid events and tremor. One possibility is to make the hypothesis of a very heterogeneous medium with highly dispersive and attenuative shallow materials and strong lateral heterogeneity. In such a medium the phase at high frequency could be laterally refracted, travelling along a path of lower attenuation, and arriving at the array site with back-azimuth and slowness different from that of the low-frequency phase. We are planning an experiment to better constrain the source position in order to better interpret this experimental evidence.

Acknowledgements

This paper has been partly supported by Gruppo Nazionale di Vulcanologia, CNR and MURST (40% and 60%) and by ANT94-0854-C02 and ANT95-0994-C03 and by Grupo de Investigacion en Geofisica J.A. 4057. We gratefully acknowledge to the Spanish Army and Navy for the logistic support in the Gabriel de Castilla Station.

Marcello Martini, F. Vidal and G. Saccorotti are acknowledged for useful discussions. During the revision process B. Chouet and S. Malone helped us in the revision of the Discussions, giving suggestions for the next seismology experiments at Deception.

REFERENCES

CAPON, J. (1969): High-resolution frequency wavenumber spectrum analysis, *Proc. IEEE*, **57** (8), 1408-1418.

CHOUET, B. (1992): A seismic model for the source of long period events and harmonic tremor in volcanic seismology, in *IAVCEI Proceedings in Volcanology*, edited by P. GASPARINI *et al.* (Springer Verlag, New York), vol. 3, 133-156.

CHOUET, B. (1996): Dynamics of a fluid driven crack in three dimensions by the finite difference method, *J. Geophys. Res.*, **91**, 13967-13992.

DEL PEZZO, E., M. LA ROCCA and J.M. IBAÑEZ (1997): Observations of high frequency scattered waves using dense arrays at Teide Volcano, *Bull. Seismol. Soc. Am.*, **87** (6), 1637-1647.

FRANKEL, A., S. HOUGH, P. FRIBERG and R. BUSBY (1991): Observations of Loma Prieta aftershocks from a dense array in Sunnyvale, California, *Bull. Seismol. Soc. Am.*, **81**, 1900-1922.

GOLDSTEIN, P. and B. CHOUET (1994): Array measurements and modeling of sources of shallow volcanic tremor at Kilauea volcano, Hawaii, *J. Geophys. Res.*, **99**, 2637-2652.

IBAÑEZ, J.M., J. MORALES, G. ALGUACIL, J. ALMENDROS, R. ORTIZ and E. DEL PEZZO (1997): Intermediate-focus earthquakes under South Shetland Islands (Antarctica), *Geophys. Res. Lett.*, **24**, 531-534.

LU, N.Q., A. PROSPERETTI and S.W. YOON (1990): Underwater noise emission from bubble clouds, *IEEE J. Oceanic Eng.*, **15**, 275-281.

MARTÌ, J., J. VILA and J. REY (1995): Deception Island (Bransfield Strait-Antartica): an example of caldera developed by extensional tectonics, *in Volcano Instability on the Earth and Other Planets*, edited by W. MCGUIRE, A. JOHNS and J. NEUBERG, *Geol. Soc. London, Spec. Publ.*, **110**, 253-265.

MARTINI, M. and L. GIANNINI (1988): Deception Island (South Shetlands): an area of active volcanism in Antarctica, *Mem. Soc. Geol. Ital.*, **43**, 117-122.

MONTALBETTI, J.R. and E.R. KANASEVICH (1970): Enhancement of teleseismic body phases with a polarization filter, *Geophys. J. R. Astron. Soc.*, **21**, 119-129.

MORI, J., J. FILSON, E. GRANSWICK, R. BORCHERT, R. AMIRBEKIAN, V. AHARONIAN and L. HACHVERDIAN (1994): Measurements of *P* and *S* wave fronts from the dense three-dimensional array at Garni, Armenia, *Bull. Seismol. Soc. Am.*, **84** (4), 1089-1096.

MORRISSEY, M.M. and B. CHOUET (1997): A numerical investigation of chocked flow dynamics and its application to the triggering mechanism of long period events at Redoubt Volcano, Alaska, *J. Geophys. Res.*, **102**, 7965-7983.

POWER, J.A., J.C. LAHR, R.A. PAGE, B.A. CHOUET, C.D. STEPHENS, D.H. HARLOW, T.I. MURRAY and J.C. DAVIES (1994): Seismic evolution of the 1989-1990 eruption sequence of Redoubt volcano, Alaska, *J. Volcanol. Geotherm. Res.*, **62**, 69-94.

SMELLIE, J.L. (1989): Deception Island, in *Tectonics of the Scotia Arc, Antartica*, edited by I.W.D. DALZIEL, Field trip guidebook T180, 28th International Geological Congress (Washington DC- AGU, 1989), 146-152.

VILA, J., R. ORTIZ, A.M. CORREIG and A. GARCÍA (1992): Seismic activity on Deception Island, in *Recent Progress in Antarctic Earth Science*, edited by Y. YOSHIDA *et al.* (Terra Scientific Publishing Company, Tokyo), 449-456.

VILA, J., A.M. CORREIG and J. MARTÌ (1995): Attenuation and source parameters at Deception Island (South Shetland Islands, Antartica), *Pageoph*, **144** (2), 229-250.